Monthly Notices
of the
ROYAL ASTRONOMICAL SOCIETY

MNRAS **483,** 1850–1861 (2019)
Advance Access publication 2018 November 12

doi:10.1093/mnras/sty2915

The census of interstellar complex organic molecules in the Class I hot corino of SVS13-A

E. Bianchi [1,2]★ C. Codella,[1,2] C. Ceccarelli,[1,3] F. Vazart,[1] R. Bachiller,[4] N. Balucani [1,2,5] M. Bouvier,[1] M. De Simone,[1] J. Enrique-Romero,[1] C. Kahane,[1,3] B. Lefloch,[1,3] A. López-Sepulcre,[1,6] J. Ospina-Zamudio,[1] L. Podio [2] and V. Taquet[2]

[1]*Univ. Grenoble Alpes, IPAG, F-38000 Grenoble, France*
[2]*INAF-Osservatorio Astrofisico di Arcetri, L.go E. Fermi 5, I-50125 Firenze, Italy*
[3]*CNRS, IPAG, F-38000 Grenoble, France*
[4]*IGN, Observatorio Astronómico Nacional, Calle Alfonso XII, E-28004 Madrid, Spain*
[5]*Dipartimento di Chimica, Biologia e Biotecnologie, Universitá degli Studi di Perugia, Via Elce di Sotto 8, I-06123 Perugia, Italy*
[6]*Institut de Radioastronomie Millimtrique (IRAM), 300 rue de la Piscine, F- 38406 Saint-Martin-d'Héres, France*

Accepted 2018 October 24. Received 2018 October 11; in original form 2018 June 15

ABSTRACT

We present the first census of the interstellar Complex Organic Molecules (iCOMs) in the low-mass Class I protostar SVS13-A, obtained by analysing data from the IRAM-30 m Large Project ASAI (Astrochemical Surveys At IRAM). They consist of a high-sensitivity unbiased spectral survey at the 1mm, 2mm, and 3mm IRAM bands. We detected five iCOMs: acetaldehyde (CH_3CHO), methyl formate ($HCOOCH_3$), dimethyl ether (CH_3OCH_3), ethanol (CH_3CH_2OH), and formamide (NH_2CHO). In addition, we searched for other iCOMs and ketene (H_2CCO), formic acid (HCOOH) and methoxy (CH_3O), whose only ketene was detected. The numerous detected lines, from 5 to 37 depending on the species, cover a large upper level energy range, between 15 and 254 K. This allowed us to carry out a rotational diagram analysis and derive rotational temperatures between 35 and 110 K, and column densities between 3×10^{15} and 1×10^{17} cm^{-2} on the 0.3 arcsec size previously determined by interferometric observations of glycolaldehyde. These new observations clearly demonstrate the presence of a rich chemistry in the hot corino towards SVS13-A. The measured iCOMs abundances were compared to other Class 0 and I hot corinos, as well as comets, previously published in the literature. We find evidence that (i) SVS13-A is as chemically rich as younger Class 0 protostars, and (ii) the iCOMs relative abundances do not substantially evolve during the protostellar phase.

Key words: Molecular data – Stars: formation – ISM: molecules – radio lines: ISM – submillimetre: ISM.

1 INTRODUCTION

The measurement of the abundance of interstellar Complex Organic Molecules (hereinafter iCOMs, C-bearing molecules containing at least six atoms; Herbst & van Dishoeck 2009; Ceccarelli et al. 2017) is one of the several pieces of the huge puzzle to complete if one wants to understand or, more humbly, to just shed light on the processes that led to the emergence of life on Earth and, possibly, on other planets. Indeed, simple organic molecules formed during the protostellar and protoplanetary disc phases might survive and be delivered to the nascent planet, providing seeds for the formation of the more complex, real prebiotic species needed to the first living beings.

In the context of Solar-type protostars and planetary systems, Class 0 hot corinos are the objects where the detection and study of iCOMs have been traditionally easier. These are compact ($\geq$100 au), hot ($\geq$100 K), dense ($\geq 10^7$ cm^{-3}), and iCOMs enriched regions at the centre of the Class 0 protostellar envelopes (e.g. Ceccarelli et al. 2007; Caselli & Ceccarelli 2012). Their chemical richness is believed to be caused by the sublimation of the icy mantles that coat the dust grains and the consequent injection into the gas-phase of species which either are themselves iCOMs (e.g. Garrod & Herbst 2006) or which react in the gas-phase and form iCOMs (e.g. Charnley, Tielens & Millar 1992; Balucani, Ceccarelli & Taquet 2015; Skouteris et al. 2017; Skouteris et al. 2018) or both.

★ E-mail: eleonora.bianchi@univ-grenoble-alpes.fr

© 2018 The Author(s)
Published by Oxford University Press on behalf of the Royal Astronomical Society

Downloaded from https://academic.oup.com/mnras/article/483/2/1850/5174973 by Biblioteca di Scienze, Università degli studi di Firenze user on 29 December 2020

From an evolutionary point of view, Class I sources represent a bridge between the Class 0 sources, characterized by a thick collapsing envelope and an embedded forming disc (Enoch et al. 2009; Tobin et al. 2015), and the Class II and III sources, characterized by the presence of a prominent circumstellar disc, where planets eventually form (Garufi et al. 2017; Avenhaus et al. 2018). However, it is not clear whether this is also valid from a chemical point of view. On the one hand, (some) Class 0 sources possess a hot corino with the detection of several iCOMs: methyl formate ($HCOOCH_3$), dimethyl ether (CH_3OCH_3), acetaldehyde (CH_3CHO), ethanol (CH_3CH_2OH), and formamide (NH_2CHO) are among the most easily detected iCOMs (see references below). On the other hand, protoplanetary discs only show emission from simpler iCOMs: methanol (CH_3OH), acetic acid (HCOOH), ethyl cyanide (CH_3CN), and cyanoacetylene (HC_3N) are the most complex molecules so far detected (Chapillon et al. 2012; Dutrey et al. 2014; Öberg et al. 2015; Walsh et al. 2016; Favre et al. 2018).

The question is: are more complex molecules not detected in protoplanetary discs only because of the current instruments detection limits or because iCOMs are not present there? In other words, does the chemical complexity vary with the evolutionary phase? One can answer this question by starting understanding whether there is any change in the chemical complexity going from Class 0 to I sources. This would provide a base to predict the chemistry at work in the later phase, the protoplanetary disc one.

Due to the new powerful facilities developed in the last decade, such as NOEMA and ALMA, several projects have now focused on the chemical composition of Class 0 hot corinos (e.g. Jørgensen et al. 2012, 2016, 2018; Maury et al. 2014; Taquet et al. 2015; Codella et al. 2016; Imai et al. 2016; De Simone et al. 2017; López-Sepulcre et al. 2017; Oya et al. 2017; Bianchi et al. 2017b; Ospina Zamudio et al. 2018). On the other hand, very little has been done so far to study the overall iCOMs composition of Class I hot corinos. Only a couple of Class I sources have been observed so far in a few iCOMs with the IRAM-30 m (Öberg, Lauck & Graninger 2014; Graninger, Wilkins & Öberg 2016; Bergner et al. 2017), and in none was a full census obtained.

We present here the first iCOMs census in a Class I source, SVS13-A. This was obtained by analysing the unbiased spectral survey of the 3, 2, and 1 mm bands observable with the IRAM-30 m, which is part of the Large Program *ASAI* (Astrochemical Surveys At IRAM, www.oan.es/asai; Lefloch et al. 2018).

The article is organized as follows: In Section 2, we present the source background; in Section 3, the observations and the line identification procedure; in Section 4, the main results for the analysis of each molecular species and in Section 5 we discuss the results. Finally, Section 6 is for the conclusions.

2 SOURCE BACKGROUND

SVS13-A is a Class I protostar located in the SVS13 cluster of the NGC 1333 cloud in Perseus, which lies at a distance of (235 ± 18) pc (Hirota et al. 2008). Next to SVS13-A lies the Class 0 protostar SVS13-B, about 15 arcsec apart (see e.g. Chini et al. 1997; Bachiller et al. 1998; Looney, Mundy & Welch 2000; Chen, Launhardt & Henning 2009; Tobin et al. 2016, and references therein).

The SVS13-A protostar has a bolometric luminosity of $L_{\rm bol} \simeq 32.5\ L_{\odot}$, a low $L_{\rm submm}/L_{\rm bol}$ ratio (∼0.8 per cent) and a bolometric temperature $T_{\rm bol} \sim 188$ K (Tobin et al. 2016). In addition, SVS13-A is associated with an extended outflow (> 0.07 pc, Lefloch et al. 1998; Codella, Bachiller & Reipurth 1999) as well as with the well-known chain of Herbig–Haro (HH) objects 7–11 (Reipurth et al. 1993). Thus, although still deeply embedded in a large-scale envelope (Lefloch et al. 1998), SVS13-A is considered a relatively evolved protostar, already entered in the Class I stage.

VLA observations have resolved SVS13-A as being a close binary system (VLA4A and VLA4B), separated by 0.3 arcsec, corresponding to ∼70 au (Rodríguez, Anglada & Curiel 1999; Anglada, Rodríguez & Torrelles 2000).

A previous analysis of the HDO lines detected in the ASAI observations revealed the presence of a hot (≥150 K), dense ($\geq 3 \times 10^7$ cm^{-3}), and compact (∼ 25 au) region, which could indicate the presence of a hot corino (Codella et al. 2016). The actual confirmation of the hot corino arrived soon after with the detection of glycolaldehyde ($HCOCH_2OH$), which emits over a ∼70 au diameter region centred on SVS13-A (De Simone et al. 2017). Subsequent higher spatial resolution observations by Lefèvre et al. (2017) found that VLA4A is associated with compact continuum emission, suggestive of a disc smaller than about 50 au. In addition, VLA4A is associated with molecular emission, indicating that it is the hot corino source. VLA4B, on the other hand, seems deprived of molecular emission but it is driving a small-scale H_2/SiO microjet.

To conclude, based on all these observations, SVS13-A seems to be a very good target where to obtain a census of the iCOMs present in a Class I hot corino.

3 OBSERVATIONS AND LINE IDENTIFICATION

3.1 Observations

Observations were performed with the IRAM-30 m telescope at Pico Veleta (Spain) in the framework of the ASAI large program (see Introduction). Briefly, ASAI provided an unbiased spectral survey of the 3 mm (80–116 GHz), 2 mm (129–173 GHz), and 1.3 mm (200–276 GHz) bands, acquired during several runs between 2012 and 2014. The rms noise (in $T_{\rm MB}$ scale) is about 2 mK, 7 mK, 9 mK in a channel of 0.6 km s^{-1}, 0.4 km s^{-1}, and 0.2 km s^{-1} for the 3, 2, and 1 mm spectral windows, respectively. The broad-band EMIR receivers were used, connected to the FTS200 backends, which provide a spectral resolution of 200 kHz. The observations were acquired in wobbler switching mode (with a 180 arcsec throw) and pointed towards SVS13-A, namely at $\alpha_{\rm J2000} = 03^{\rm h}29^{\rm m}03\overset{\rm s}{.}76$, $\delta_{\rm J2000} = +31^{\circ}16'03\overset{''}{.}0$. The pointing was found to be accurate to within 3 arcsec. The telescope Half Power Beam Widths (HPBWs) lie from ≃9 arcsec at 276 GHz to ≃30 arcsec at 80 GHz. For a more detailed description of the ASAI observations we refer the reader to Lefloch et al. (2018).

The data reduction was performed using the GILDAS–CLASS[1] package. The uncertainty of the calibration varies between ∼10 per cent at 3 mm and ∼20 per cent at 1 mm. Finally, the line intensities were converted from antenna temperature to main beam temperature ($T_{\rm MB}$), using the main beam efficiencies reported in the IRAM-30 m website.[2]

3.2 Line identification and spectroscopic properties

Line identification was performed using the ULSA (Unbiased Line Spectral Analysis) package developed at IPAG. ULSA allows to automatically identify lines in the ASAI spectra using the Jet Propulsor

[1] *http://www.iram.fr/IRAMFR/GILDAS*
[2] *http://www.iram.es/IRAMES/mainWiki/Iram30mEfficiencies*

Downloaded from https://academic.oup.com/mnras/article/483/2/1850/5174973 by Biblioteca di Scienze, Università degli studi di Firenze user on 29 December 2020

Laboratory (JPL,[3]Pickett et al. 1998) and Cologne Database for Molecular Spectroscopy (CDMS[4], Müller et al. 2001; Müller et al. 2005) molecular line data bases. We excluded from the analysis those lines peaking at velocities displaced with respect to the systemic velocity by more than 0.6 km s^{-1}, to minimize effects due to line blending.

We looked for the iCOMs commonly detected so far towards low-mass hot corinos. More specifically, we searched for lines from acetaldehyde (CH_3CHO), methyl formate ($HCOOCH_3$), dimethyl ether (CH_3OCH_3), ethanol (CH_3CH_2OH), propynal (HC_2CHO), glycoaldehyde ($HCOCH_2OH$), methylamine (CH_3NH_2), and acetone (CH_3COCH_3). We also added some important iCOMs precursors such as ketene (H_2CCO), formic acid (HCOOH), and methoxy (CH_3O).

We summarize here the spectroscopic properties of some species. Because of the symmetries due to the presence of a methyl group (CH_3), CH_3CHO, $HCOOCH_3$, and CH_3CH_2OH are associated with the *A*-type and *E*-type forms, while CH_3OCH_3, having two methyl groups, can be found in four forms (*AA*, *AE*, *EA*, *EE*). The spin statistical weights of the *A* and *E* type levels is the same (Turner 1991 and references therein). The spin statistical weight of the (*AA*, *AE*, *EA*, *EE*) type levels are 6 (*AA*), 16 (*EE*), 2 (*AE*), 4 (*EA*), and 10 (*AA*), 16 (*EE*), 6 (*AE*), 4 (*EA*) for ee-oo and eo-oe rotational transitions,[5] respectively (Myers & Bright Wilson 1960).

In the case of ethanol (CH_3CH_2OH), the internal rotation is negligible in most instances. However, ethanol exists under the form of three rotamers: anti, gauche +, and gauche − (see Section 4.6 and Fig. B1).

Finally, H_2CCO exists in two isomers, ortho (transition with *K* odd) and para (transitions with *K* even), that have different nuclear spin states. For kinetic temperature much larger than 15 K, the ortho-to-para ratio is expected to be close to the statistical value of 3 (e.g. Ohishi et al. 1991).

4 RESULTS

4.1 Overview

Table 1 summarizes the list of the iCOMS detected in SVS13-A, with the number of identified lines and their upper level energy E_u ranges. We detected more than 100 lines with E_u up to 254 K emitted by H_2CCO, CH_3CHO, $HCOOCH_3$, CH_3OCH_3, and CH_3CH_2OH. The considered detection limit is 3σ in the integrated intensity.

We fitted the detected lines with a Gaussian function using the GILDAS–CLASS software. Their spectral parameters as well as the results from the Gaussian fits are presented in Tables C1, C2, C3, C4, C5. Examples of the detected line profiles (in T_{MB} scale) are shown in Fig. 4.1. The peak velocities of the detected lines are between +8 and + 9 km s^{-1}, consistent, within the uncertainties, with the systemic velocity of both SVS13-A and SVS13-B (+ 8.6 km s^{-1}, Chen et al. 2009; López-Sepulcre et al. 2015). However, we note that the vast majority of the iCOMs lines are detected in the 1.3 mm band, namely with a beam whose HPBW is ∼10 arcsec. Therefore, the detected iCOMs emission is mostly from SVS13-A and the contribution from SVS13-B will be neglected in the following analysis. As regard the methyl formate lines, the noise on the spectra is too large hampering a more sophisticated analysis. Specifically, the sometime apparent double peaks are always within the noise of the spectrum, as well as possible wings. For this reason, we decided to not push further the analysis.

Having lines with a large E_u range can be used to identify different regions in the field of view that have different excitation conditions (density and temperature). For example, using a non-LTE analysis of methanol lines towards SVS13-A we disentangled their emission from the envelope and the hot corino, respectively (Bianchi et al. 2017a). Unfortunately, the collisional rates for the observed iCOMs transitions are not available in literature, so that we used the standard Rotational Diagram (RD) analysis to estimate the temperature and the column density. Yet, even in this case, the occurence of multiple components would be visible in the RD as straight lines with different slopes.

To construct the RD of each detected species, we included also lines that consist of several transitions with the same upper level energy, but different Einstein coefficients and statistical weights. In this case, we adopted the formalism described in Appendix A (see the online material).

As a first step, we performed the RD analysis without beam filling factor corrections. The obtained rotational temperatures are: (240 ± 95) K for H_2CCO, (50 ± 10) K for CH_3CHO, (400 ± 200) K for $HCOOCH_3$, (110 ± 10) K for CH_3OCH_3, (140 ± 60) K for NH_2CHO, and (100 ± 30) K for CH_3CH_2OH. The obtained values, always higher than 50 K, implies that the iCOMs emission is very likely dominated by the hot corino of SVS13-A. Therefore, in the subsequent analysis, we assume a source size of 0.3 arcsec for all iCOMs, based on the interferometric observations of the $HCOCH_2OH$ emission by De Simone et al. (2017) and on the non-LTE analysis of the $^{13}CH_3OH$ lines (Bianchi et al. 2017a). Table 1 reports the list of the derived rotational temperatures and column densities for each detected species. The next subsection describes the results for each detected iCOM as well as some general considerations and comparison with previous observations.

4.2 Ketene

Ketene (H_2CCO), a near-prolate asymmetric top rotor, is one of the numerous carbon-chain molecules that were observed in the interstellar medium. It was discovered for the first time by Turner (1977). Although it is not an iCOM in the strict sense (it has only 5 atoms), it is thought to be involved in grain-surface reactions to form iCOMs such as formic acid, ethanol, and acetaldehyde (Charnley, Tielens & Rodgers 1997; Garrod, Widicus Weaver & Herbst 2008; Hudson & Loeffler 2013 and references therein), so we considered it in this study.

We detected six lines of the para and 11 of the ortho form of H_2CCO, respectively. Five of the detected transitions are in the 2 mm band, namely they are observed with a HPBW of ∼15 arcsec, while the rest of the lines are detected in the 1.3 mm band (HPBW ∼10 arcsec). The line upper level energies (E_u) are in the 40–206 K range. The observed spectra are shown in Fig. C1, while the fit to the spectral line parameters are reported in Table C1.

The line profiles are close to a Gaussian with full width at half-maximum (FWHM) between 0.9 and 4.1 km s^{-1}. The peak velocities are close to the systemic source velocity (with values between +7.6 and + 8.9 km s^{-1}). The two transitions $8_{3,5}$–$7_{3,4}$ and $8_{3,6}$–$7_{3,5}$ with E_u = 152 K, as well as the two transitions $13_{3,10}$–$12_{3,9}$ and $13_{3,11}$–$12_{3,10}$ with E_u = 206 K, are blended (see Table C1). These lines are therefore excluded from the subsequent analysis.

[3]https://spec.jpl.nasa.gov/

[4]http://www.astro.uni-koeln.de/cdms/

[5]e (even) and o (odd) refer to the K_a, K_c labels of the energy states of an asymmetric rotor.

Downloaded from https://academic.oup.com/mnras/article/483/2/1850/5174973 by Biblioteca di Scienze, Università degli studi di Firenze user on 29 December 2020

Table 1. List of the detected iCOMs (upper half table) and upper limits of the non-detected ones (lower half table) towards SVS13-A.

Species	$N^a_{\rm lines}$	$E_{\rm u}$ (K)	$T^b_{\rm rot}$ (K)	$N^b_{\rm tot}$ (cm^{-2})	$X^c_{\rm H2}$
$^{13}CH_3OH^d$	18	20–175	100(10)	$10(2) \times 10^{16}$	3×10^{-8}
H_2CCO	13	40–206	65(10)	$13(3) \times 10^{15}$	4×10^{-9}
CH_3CHO	13	61–108	35(10)	$12(7) \times 10^{15}$	4×10^{-9}
$HCOOCH_3$	37	20–149	66(5)	$13(1) \times 10^{16}$	4×10^{-8}
CH_3OCH_3	11	33–254	110(10)	$14(4) \times 10^{16}$	5×10^{-8}
CH_3CH_2OH	5	35–137	105(60)	$11(5) \times 10^{16}$	4×10^{-8}
NH_2CHO^e	13	15–102	45(8)	$26(9) \times 10^{14}$	9×10^{-10}
			Upper limits^f		
HCOOH	–	–	80	$\leq 5 \times 10^{15}$	$\leq 2 \times 10^{-9}$
HC_2CHO	–	–	80	$\leq 1 \times 10^{16}$	$\leq 3 \times 10^{-9}$
$HCOCH_2OH$	–	–	80	$\leq 8 \times 10^{15}$	$\leq 3 \times 10^{-9}$
CH_3NH_2	–	–	80	$\leq 1 \times 10^{16}$	$\leq 3 \times 10^{-9}$
CH_3COCH_3	–	–	80	$\leq 1 \times 10^{16}$	$\leq 3 \times 10^{-9}$
CH_3O	–	–	80	$\leq 3 \times 10^{15}$	$\leq 1 \times 10^{-9}$

Notes. [a]Number of lines used in the analysis. Additional detected transitions, excluded from the analysis because contaminated, are reported in Appendix C, available online.
[b]Parameters are derived for a source size of 0.3 arcsec, as measured by De Simone et al. (2017).
[c]We assume $N(H_2) = 3 \times 24$ cm^{-2} from Chen et al. (2009) (see Sec. 5.1 for details).
[d]From Bianchi et al. (2017a).
[e]We repeated the analysis previously reported by López-Sepulcre et al. (2015), which was obtained assuming a source size of 1 arcsec instead of 0.3 arcsec.
[f]To derive the upper limit to the column density of each non-detected species we assumed $T_{\rm rot}$ equal to 80 K. The upper limits refer to 1σ.

In Fig. 2, we show the RD of both ortho and para transitions. Their distribution does not show any significant scatter from a common linear fit, within the errors. In other words, the RD is consistent with the high-temperature LTE limit o/p statistical values of 3. We found a rotational temperature $T_{\rm rot} = (65 \pm 10)$ K and a column density $N_{\rm tot} = (13 \pm 3) \times 10^{15}$ cm^{-2} (Table 1).

4.3 Acetaldehyde

Acetaldehyde (CH_3CHO), an asymmetric top molecule, was detected in many star formation environments, from cold dark cores (e.g. Bacmann et al. 2012; Cernicharo et al. 2012, Vastel et al. 2014; Jiménez-Serra et al. 2016) to hot corinos (e.g. Cazaux et al. 2003; Codella et al. 2016) and protostellar shocks (e.g. Codella et al. 2015; Lefloch et al. 2017). Despite the several detections in a large range of interstellar conditions, it is not clear yet if acetaldehyde is synthesized directly on the grain surfaces (e.g. Garrod & Herbst 2006) or via gas-phase reactions (e.g. Charnley 2004). In particular, the first route was recently questioned by quantum chemistry calculations (Enrique-Romero et al. 2016) but the picture is still far from being clear.

We detected six transitions of CH_3CHO in the E form and 10 transitions in the A form, respectively. All the lines are detected in the 1 mm band.[6] The line upper level energies range from 16 to 108 K while the peak velocities are consistent with the systemic velocity with values between +7.8 and + 9.0 km s^{-1}. The line shape is nearly Gaussian with FWHMs of ∼2–4 km s^{-1}. The spectral parameters and the Gaussian fit results are reported in Table C2, while the spectra of the detected lines are shown in Fig. C2. The CH_3CHO $12_{3,9}$–$11_{3,8}$ A transition was also excluded from the analysis since it is contaminated by the CH_2DOH $9_{2,7}$–$9_{1,8}$ e0 transition (see Bianchi et al. 2017a). The RD analysis, shown in Fig. 2, indicates a rotational temperature $T_{\rm rot} = (35 \pm 10)$ K and a column density $N_{\rm tot} = (12 \pm 7) \times 10^{15}$ cm^{-2}.

4.4 Methyl formate

Another important iCOM that appears to be common in star-forming regions is methyl formate ($HCOOCH_3$), an asymmetric top species. It was observed towards Sgr B2 by Brown et al. (1975) and then detected in both cold environments (e.g. Bacmann et al. 2012; Cernicharo et al. 2012; Jiménez-Serra et al. 2016; Taquet et al. 2017), in hot corinos (e.g. Cazaux et al. 2003; Bottinelli et al. 2004) and protostellar shocks (Arce et al. 2008; Lefloch et al. 2017). Methyl formate is the most abundant among its isomers acetic acid (CH_3COOH) and glycolaldehyde ($HCOCH_2OH$). In the Sgr B2 complex, a glycolaldehyde : acetic acid : methyl formate relative abundance of ∼0.5:1:26 was measured by Hollis et al. (2001). The reason of this abundance differentiation is still unclear but it is thought to be related to the respective formation processes (e.g. Bennett & Kaiser 2007, but see also Lattelais et al. 2009). It is not clear how methyl formate is synthesized. It could be a grain-surface (e.g. Chuang et al. 2017 and references therein) or a gas-phase (Balucani et al. 2015; Taquet, Wirström & Charnley 2016) reactions product.

Methyl formate can exist in two different geometrical configurations: the *cis* configuration, if the methyl group (CH_3) is on the same side of the carbon chain; the *trans* configuration if the methyl group is on opposing sides of the carbon chain. The *trans* form is less stable than the *cis* form and, at a temperature of 100 K, the population ratio of *cis* over *trans* is ∼10^{13}:1 (Neill et al. 2012). Furthermore, the involved energy barriers make unlikely the in-

[6]The $5_{1,5}$–$4_{1,4}$ E transition is detected in the 3 mm band, but it has been excluded from the analysis because it is contaminated by an unidentified emission line.

Downloaded from https://academic.oup.com/mnras/article/483/2/1850/5174973 by Biblioteca di Scienze, Università degli studi di Firenze user on 29 December 2020

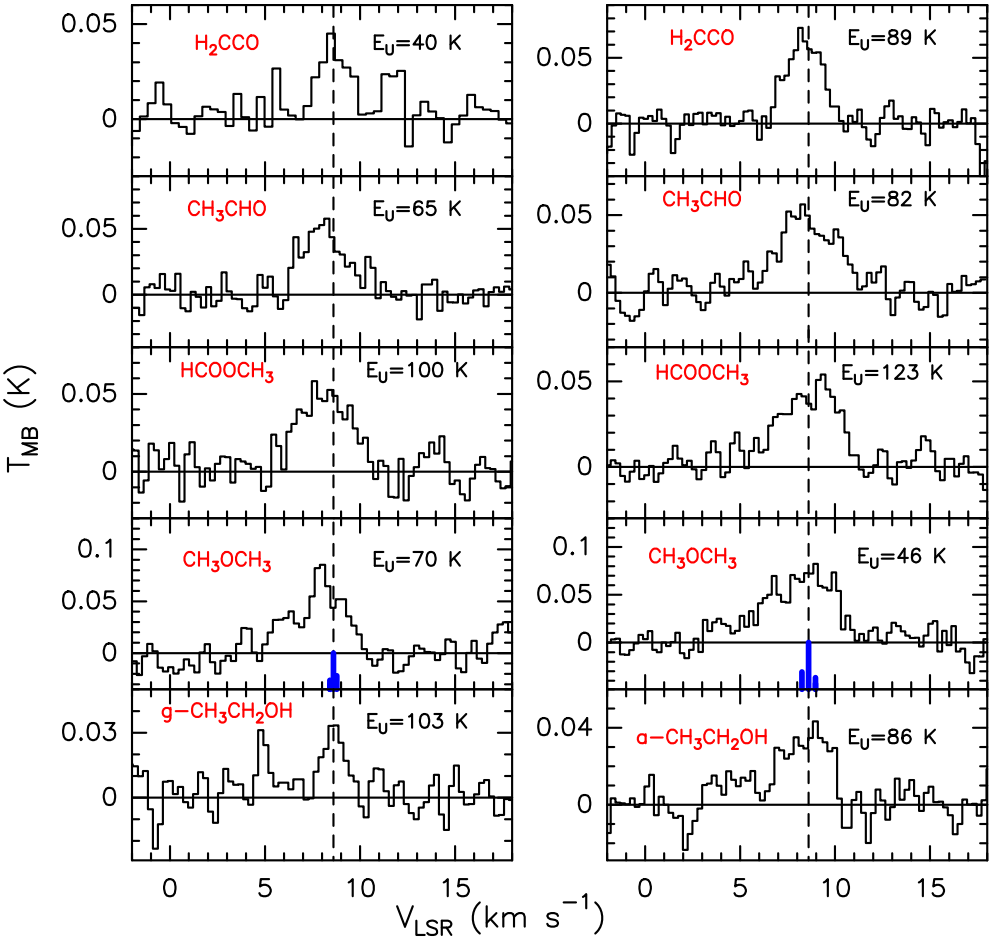


Figure 1. Examples of the observed spectra, in T_{MB} scale (i.e. not corrected for the beam dilution): species and excitation energies are reported in the upper left and right corner of each panel, respectively. The vertical dashed line stands for the ambient LSR velocity (+ 8.6 Km s^{-1}; Chen et al. 2009). In the CH_3OCH_3 panels, the blue lines indicate the presence of blended transitions with the same upper level energy. The complete observed spectra for each species are reported in Appendix C and they are available online.

terconversion between *cis* and *trans* forms in interstellar environments, which explains why only the *cis* was detected (Laas et al. 2011).

We detected in total 37 lines of $HCOOCH_3$. Among them, only one line was detected in the 3 mm band (with a HPBW ∼27 arcsec) while 11 lines are detected in the 2 mm band and the others in the 1 mm band (namely with HPBWs of ∼15 arcsec and ∼10 arcsec, respectively). The lines cover a large range of upper level energies E_u, from 20 K to 158 K. The line profiles are close to Gaussian shape with typical FWHM∼2–4 km s^{-1} and the peak velocities are close to the systemic source velocity with values between +7.5 and + 9.2 km s^{-1}. The spectral line parameters and the results of the Gaussian fit are reported in Table C3 while the emission line spectra are shown in Fig. C3.

The RD analysis gives a rotation temperature T_{rot} = (66 ± 5) K and a column density N_{tot} = (13 ± 1) × 10^{16} cm^{-2}, as illustrated in Fig. 2 and reported in Table 1. Note that in some cases, because of the limited spectral resolution, we observe only one line but it consists of different transitions with the same upper level energy E_u. These unresolved multiplets are treated in the rotation diagram analysis using the method illustrated in Appendix A1 (see the online matherial). On the other hand, the lines containing several transitions with different upper level energies and different quantum numbers are excluded from the analysis.

4.5 Dimethyl ether

Dimethyl ether (CH_3OCH_3) is one of the largest iCOMs detected in the interstellar medium and, similar to others, it seems to be present in all the stages of the star formation process. Dimethyl ether was detected for the first time by Snyder et al. (1974) in the Orion nebula and successively, in the context of Sun-like star-forming regions, in different hot corinos (e.g. Cazaux et al. 2003, Bottinelli et al. 2004) as well as in cold prestellar cores (e.g. Bacmann et al. 2012; Cernicharo et al. 2012; Jiménez-Serra et al. 2016). As for other iCOMs, dimethyl ether is predicted to be formed either on the grain surfaces (e.g. Cuppen et al. 2017 and references therein) or in the gas phase (Balucani et al. 2015, Skouteris et al. 2019 G105).

Dimethyl ether is an asymmetric top molecule with two equivalent methyl groups. The torsional movements along the CO-bond of the two CH_3 rotors, cause the splitting of each rotational level into four substates AA, EE, EA, and AE.

We detected 11 lines of dimethyl ether, with upper level energies ranging from 33 to 254 K. All the detected lines consist of several lines not spectrally resolved (see Table C4). As a consequence,

Downloaded from https://academic.oup.com/mnras/article/483/2/1850/5174973 by Biblioteca di Scienze, Università degli studi di Firenze user on 29 December 2020

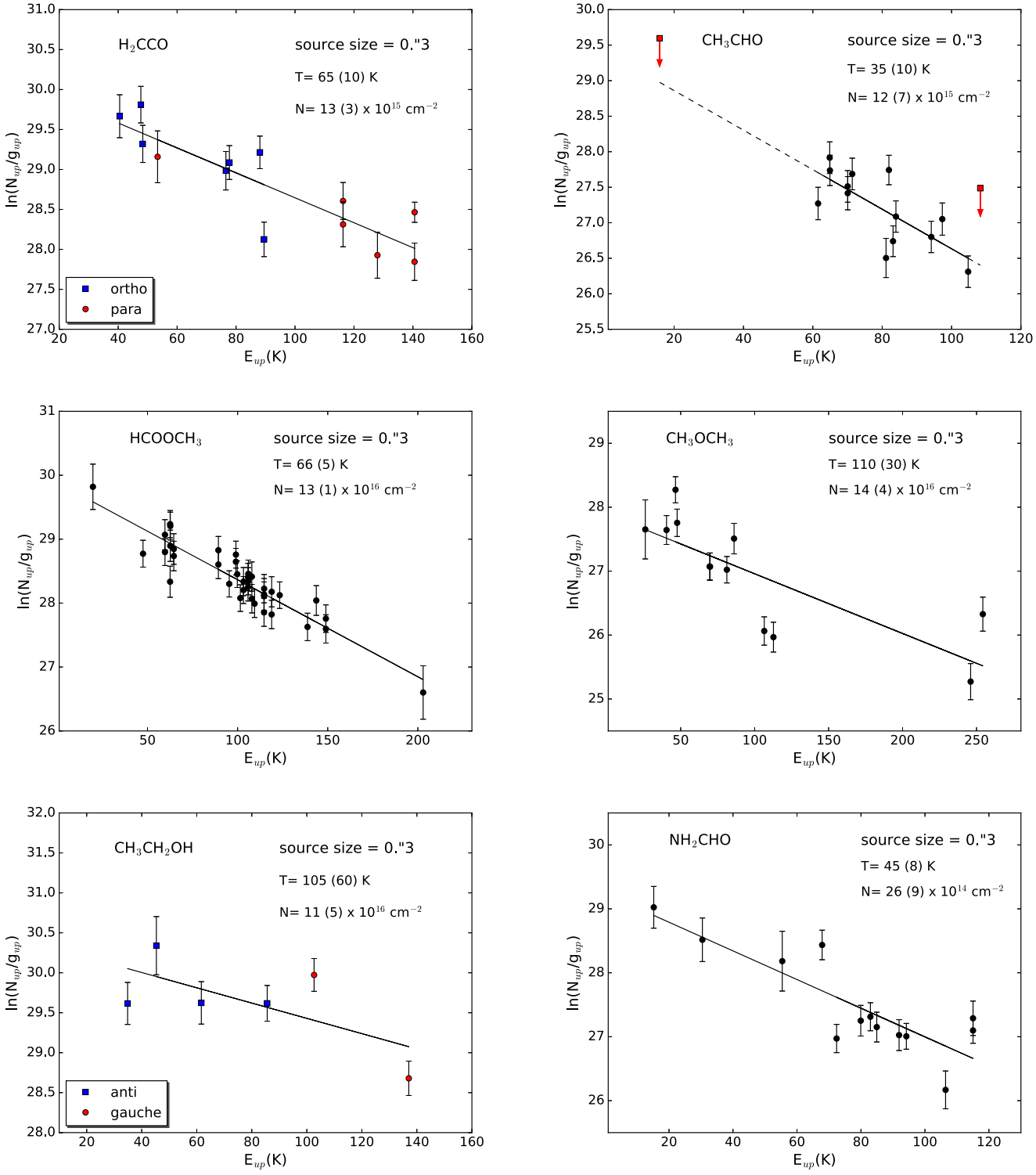


Figure 2. Rotationdiagrams of ketene (upper left-hand panel), acetaldehyde (upper right-hand panel), methyl formate (left middle panel), dimethyl ether (right middle panel), ethanol (lower left-hand panel), and formamide (lower right-hand panel). An emitting region size of 0.3 arcsec (corresponding to ∼70 au) is assumed (see the text). The parameters N_u, g_u, and E_u are the column density, the degeneracy, and the energy (with respect to the ground state of each symmetry) of the upper level, respectively. The derived values of the rotational temperature and the column density are reported in each panel for each species. For H_2CCO, the blue squares and red dots indicate ortho- and para- transitions, respectively. The red arrows in the CH_3CHO panel indicate the $5_{1,5}$–$4_{1,4}$ E and $12_{4,8}$–$11_{4,7}$ E transitions, which were not used in the fit because contaminated. For CH_3CH_2OH, the blue squares and red dots indicate anti- and gauche- transitions, respectively. NH_2CHO data are from López-Sepulcre et al. (2015) but they were reanalysed assuming the size of 0.3 arcsec.

Downloaded from https://academic.oup.com/mnras/article/483/2/1850/5174973 by Biblioteca di Scienze, Università degli studi di Firenze user on 29 December 2020

the line profiles do not show a Gaussian shape. For this reason, we do not perform a Gaussian fit but instead we considered the velocity-integrated intensity over the interval where the lines are expected to emit (Table C4). We perform the RD analysis treating the multiplets with the method described in Appendix A1 (see the online matherial). To be consistent, we use only the lines composed by any of the four forms (AA, AE, EE, EA) merged in one line. The values derived for the rotation temperature and column density are $T_{\rm rot} = (110 \pm 10)$ K and $N_{\rm tot} = (14 \pm 4) \times 10^{16}$ cm^{-2}, respectively (see Fig. 2 and Table 1).

4.6 Ethanol

Ethanol (CH_3CH_2OH) was detected for the first time in space in 1975, towards Sgr B2 (Zuckerman et al. 1975), and successively in several high- and low-mass star-forming regions. Recently a correlation was observed between ethanol and glycolaldehyde in Sun-like protostars (Lefloch et al. 2017).

Since the information in the literature is old, we performed new quantum chemistry computations (the details are reported in Appendix B, available online.) in order to characterize the energy diagram of the three ethanol rotamers (anti, gauche + and gauche-). Fig. B1 shows their relative energies as well as the interconversion path between them. Our new computations give an energy difference between the anti and gauche forms of 71 K, slightly larger than the 56 K value by Pearson, Brauer & Drouin (2008). Therefore, for large enough temperatures (i.e. $\geq$70 K), the abundance ratio between the anti and gauche forms is equal to the respective statistical weight ratio, namely 1.

We detected two lines of the gauche and three lines of the anti forms. All the transitions are detected in the 1.3 mm band (HPBW $\simeq$ ∼10–11 arcsec). The upper level energies of the detected lines are in the 35–137 K range. The line shape is nearly Gaussian with FWHMs ranging between 1 and 3 km s^{-1}. The peak velocities are in the +8.2– + 8.6 km s^{-1} range, consistently with the systemic source velocity. The observed spectra are shown in Fig. C5, while the spectral line parameters are reported in Table C5. The RD analysis gives a rotation temperature $T_{\rm rot} = (105 \pm 60)$ K and a column density $N_{\rm tot} = (11 \pm 5) \times 10^{16}$ cm^{-2} (Fig. 2 and Table 1). The low number of detected lines and their respective upper level energies do not allow us to put strong constraints on the anti and gauche abundance ratio, so that we assumed the theoretical high-temperature limit.

4.7 Formamide

Finally, for comparison, we analysed also the lines from formamide, previously reported by López-Sepulcre et al. (2015). Formamide is an interstellar molecule of great interest because it was proposed as a prebiotic precursor of genetic material (e.g. Saladino et al. 2012, and references therein). It was detected for the first time in space by Rubin et al. (1971) towards Sgr B2, and only very recently it was reported in the context of low-mass star formation: namely protostellar shocks (Yamaguchi et al. 2012; Mendoza et al. 2014), and hot corinos (Kahane et al. 2013; López-Sepulcre et al. 2015; Coutens et al. 2016).

We detected 13 lines and analysed them using the RD approach, assuming here a size of 0.3 arcsec, as for the other species, instead of the 1 arcsec assumed by López-Sepulcre et al. (2015). The derived values of rotation temperature and column density are $T_{\rm rot} = (45 \pm 8)$ K and $N_{\rm tot} = (26 \pm 9) \times 10^{14}$ cm^{-2}, respectively (see Table 1).

4.8 Summary of the results

The summary of the derived iCOMs column densities and rotational temperatures is given in Table 1. In addition, Table 1 reports the upper limits on the column density of non-detected iCOMs detected in some Class 0 hot corinos (e.g. Jaber et al. 2014): HCOOH, HCCCOH, $HCOCH_2OH$, CH_3NH_2, CH_3COCH_3, and CH_3O. Note that, to derive the upper limits, we assumed a rotational temperature of 80 K, i.e the average temperature measured using the detected iCOMs and a typical FWHM of 2.5 km s^{-1}. We also notice that $HCOCH_2OH$ was previously imaged towards SVS13-A by De Simone et al. (2017) using the IRAM-NOEMA interferometer. These authors derived a column density $N_{\rm tot} = (21 \pm 8) \times 10^{14}$ cm^{-2}, consistent with the upper limit derived here.

With the exception of acetaldehyde and formamide, all detected iCOMs have a rotational temperature larger than about 45 K, indicating that the gas of the hot corino region dominates the line emission of these species. The lower temperature derived for acetaldehyde and formamide could indicate that there is a non-negligible emission from colder and more extended gas, but always within the 10 arcsec region where the lines were detected. It is possible that this gas is associated with the outflow. Indeed, these species were detected towards the L1157 outflow by Mendoza et al. (2014), Codella et al. (2014, 2016, 2017), and Lefloch et al. (2017).

Regarding the column densities, methyl formate, dimethyl ether, and ethanol are the detected iCOMs with the largest (and similar) values, followed by ketene and acetaldehyde (similar values) about a factor 10 lower, and then formamide, which is the least abundant detected iCOM in SVS13-A, about a factor three lower.

5 DISCUSSION

5.1 The hot corino of SVS13-A

The hot corino phenomenon was discovered about 15 yr ago towards the Class 0 protostar IRAS16293–2422 (Cazaux et al. 2003). Since then, less than 15 hot corinos were found, some of which are rather candidates than confirmed hot corinos (see later). Most of them are in Class 0 protostars: NGC 1333 IRAS4A (Bottinelli et al. 2004); IRAS4B and IRAS2A (Bottinelli et al. 2007); Serpens SMM1 and SMM4 (Öberg et al. 2011); SVS 4–5 (Öberg et al. 2014); IRAS23238 + 7401, L1455 SMM1 and B1-c (Bergner et al. 2017); HH212-mm (Codella et al. 2016); IRAS19347 + 0727 in B335 (Imai et al. 2016) L483 (Oya et al. 2017); CepE-mm (Ospina Zamudio et al. 2018). Even fewer hot corino candidates have so far been found in Class I sources: B1-a (Öberg et al. 2014) and IRAS03245 + 3002 (or L1455 IRS 1; Bergner et al. 2017) in Perseus. We notice, though, that all Class I hot corinos were observed with the single-dish IRAM-30 m telescope and that the derived rotational temperatures of the few detected iCOMs are very low, less than 20 K. These low temperatures cast some doubts on whether the detected iCOMs emission originates in the hot corinos of these sources or rather in a more extended component, such as outflows or PDRs (Photo-Dissociation Regions).

The case of SVS13-A, here studied, is a clear-cut Class I hot corino for the following reasons: (1) eight iCOMs were detected (the seven detected by this study, see Table 1, plus glycolaldehyde detected by De Simone et al. 2017); (2) the emission from one iCOM was imaged and showed to originate in a compact region (De Simone et al. 2017); (3) the rotational temperatures of the iCOMs here detected are all larger than 45 K (with the exception of acetaldehyde, which however is also the species with the smallest

Downloaded from https://academic.oup.com/mnras/article/483/2/1850/5174973 by Biblioteca di Scienze, Università degli studi di Firenze user on 29 December 2020

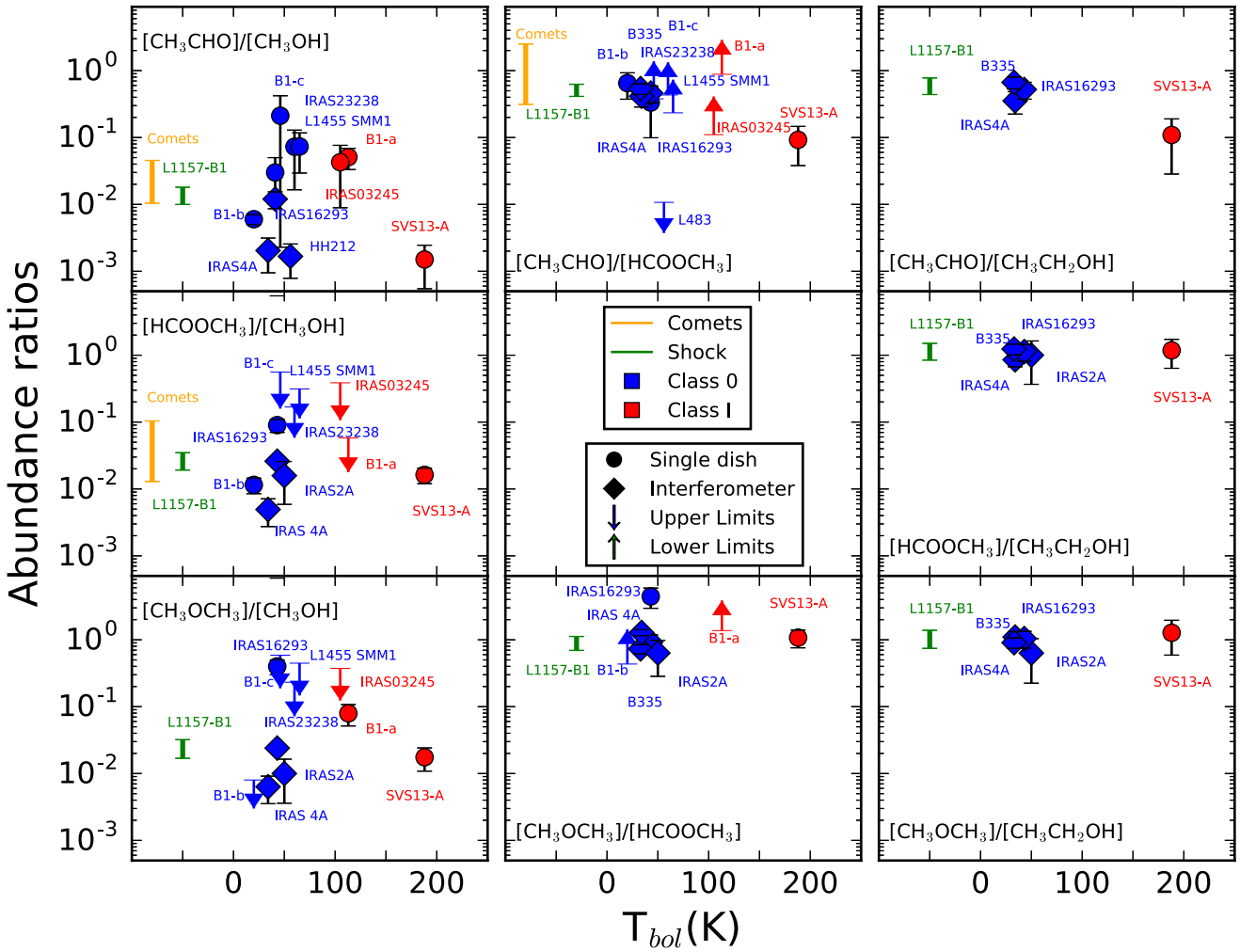


Figure 3. Abundance ratios of the iCOMs detecetd in SVS13-A compared to different sources, as indicated in the upper panels. The sources are: the pre-protostar hydrostatic core B1-b (Pezzuto et al. 2012; Gerin et al. 2015); the Class 0 sources IRAS4A, IRAS2A (Taquet et al. 2015; López-Sepulcre et al. 2017), IRAS16293–2422 (e.g. Jaber et al. 2014; Jørgensen et al. 2016, 2018), B1-c (Öberg et al. 2014; Bergner et al. 2017), IRAS23238 + 7401 (Graninger et al. 2016; Bergner et al. 2017), L1455 SMM1 (Graninger et al. 2016; Bergner et al. 2017), HH212 (Bianchi et al. 2017b; Codella et al. 2018), IRAS19347 + 0727 in B335 (Imai et al. 2016) and L483 (Oya et al. 2017); the protostellar shock L1157-B1 (Codella et al. 2010; Lefloch et al. 2017), the Class I sources B1-a (Öberg et al. 2014; Bergner et al. 2017), IRAS03245 + 3002 (Graninger et al. 2016; Bergner et al. 2017) and SVS13-A (this work); comets (Le Roy et al. 2015). The blue symbols indicate Class 0 protostars while red symbols are for Class I protostars. The circles indicate single-dish measurements while diamonds are for interferometric measurements. The arrows indicate upper limit measurements. The abundance ratios of comets and the protostellar shock L1157-B1 are reported for comparison using an orange line and a green line, respectively. Note that in these cases the x-value has no meaning.

interval of the transition upper level energy, from 61 to 108 K), which ensures that the emission arises from hot gas. In other words, SVS13-A is the only confirmed Class I hot corino and it is also the one with the largest number of detected iCOMs.

In Section 4, we derived the iCOMs column densities from the ASAI observations. In order to convert them into abundances, we estimated the H_2 column density from the IRAM-PdBI[7] continuum observations obtained by Chen et al. (2009). These authors quote a gas mass of (0.75 ± 0.12) $M_\odot$ for SVS13-A over a 1.1 arcsec diameter. Correcting for the different distance assumed by Chen et al. (2009) (350 pc instead of 235 pc, see Section 2) and the gas temperature (they assumed 20 K) gives an average H_2 density of $\sim 2.9 \times 10^9$ cm^{-3}. Therefore, assuming that the mass is mostly concentrated towards the hot corino, we obtain a H_2 column density of $\sim 3 \times 10^{24}$ cm^{-2}. The measured abundance of the iCOMs detected in SVS13-A ranges from $\sim 9 \times 10^{-10}$ (formamide) to $\sim 4 \times 10^{-8}$ (methyl formate and ethanol). The comparison of these values with those previously derived in Class 0 hot corinos is discussed in the next section.

5.2 Comparison with other hot corinos

The question that we want to address in this section is whether the SVS13-A hot corino shows any sign of diversity with respect to Class 0 hot corinos, which may indicate an evolution of the chemical composition. To this end, we compared the iCOMs abundances in the known hot corinos. We included in the comparison all candidate Class 0 and I hot corinos identified in the literature, including those observed only with single-dish telescopes. Note that, given the well-known relatively large uncertainty in the derivation of the

[7]IRAM Plateau de Bure Interferometer: *http://www.iram-institute.org/*.

Downloaded from https://academic.oup.com/mnras/article/483/2/1850/5174973 by Biblioteca di Scienze, Università degli studi di Firenze user on 29 December 2020

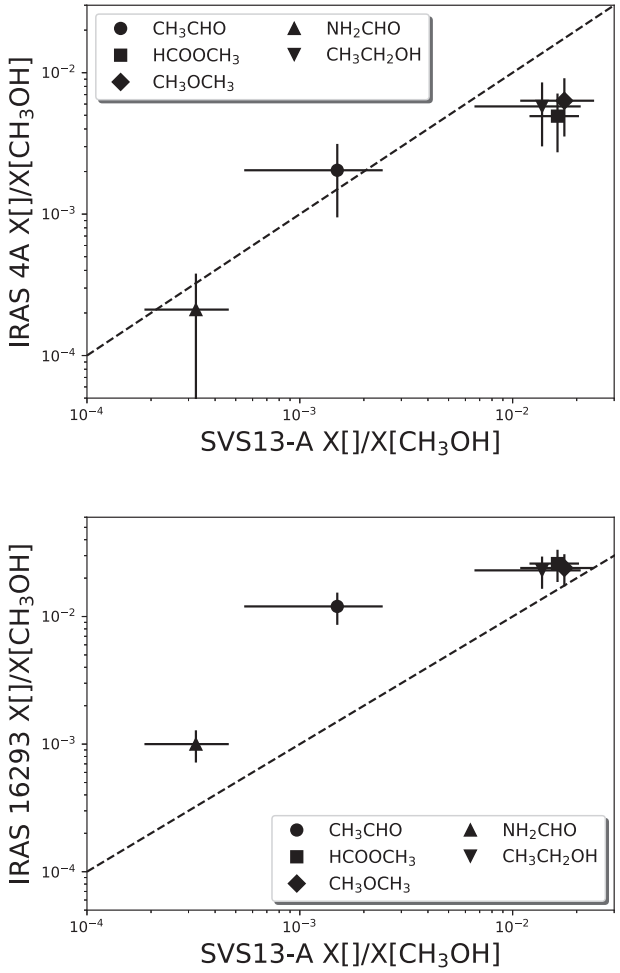


Figure 4. Abundances, normalized to methanol, of the iCOMs detected in the hot corinos of IRAS4A (upper panel, *y*-axis), IRAS16293–2422 (lower panel, *y*-axis), and SVS13-A (*x*-axis). The different symbols represent different molecules, as marked in the figure inset: acetaldehyde (circles), methyl formate (squares), dimethyl ether (diamonds), formamide (up-triangles), and ethanol (low-triangles). The iCOMs abundances in IRAS4A are from López-Sepulcre et al. (2017) and Taquet et al. (2015), those of IRAS16293–2422 are from Jørgensen et al. (2018) and Coutens et al. (2016) while the SVS13-A abundances are from this work.

H_2 column density and, hence, absolute abundances, we compared iCOMs abundance ratios of different species.

Fig. 3 shows the ratio of acetaldehyde, methyl formate, and dimethyl ether with respect to methanol, methyl formate, and ethanol, respectively. These species were selected because they are the ones detected in the largest number of candidate hot corinos. Note that the abundance ratios are showed as a function of the source bolometric temperature T_{bol}, which is considered an indicator of the different evolutionary status of the source (Myers et al. 1998).

We will conservatively limit our analysis to the objects for which the sizes of the hot corino have been determined using an interferometer: namely the Class 0 IRAS16293–2422, IRAS4A, IRAS2A, and HH212, and the Class I SVS13-A. The observations of SVS13-A, even if single-dish, are supported by the previous image of the hot corino by De Simone et al. (2017). This allows us to safely correct for the appropriate filling factor, obtaining reliable measurements of the iCOMs abundances. Fig. 3 does not show a significant difference in the iCOMs relative abundances of the four Class 0 hot corinos with respect to the (only) Class I one, SVS13-A. This is also shown in Fig. 4, where the abundances, normalized with respect to methanol, of the six iCOMs detected in SVS13-A are compared with those detected in IRAS4A and IRAS16293–2422[8] (Taquet et al. 2015; Coutens et al. 2016; López-Sepulcre et al. 2017; Jørgensen et al. 2018). In practice, the six iCOMs have similar abundance ratios, within one order of magnitude, in both Class 0 and Class I hot corinos.

We conclude that, so far based on only less than a handful sources and molecules, Class 0 and Class I hot corinos do not differ in their iCOMs relative abundances. Needless to say, more observations of both hot corinos and iCOMs are necessary to confirm or invalidate this conclusion. In this respect, it is worth noticing that the molecular deuteration seems, on the other hand, to decrease from Class 0 to Class I sources (Bianchi et al. 2017a). Also in this case, however, more measurements, especially with interferometers able to disentangle the various components in a single-dish telescope beam, are needed before drawing firm conclusions.

5.3 Comparison with comets

An important open question of astro- and cosmo-chemistry is whether there is a link between the molecules formed in the protostellar phase and, particularly, in the hot corino and those found in cometary material (see e.g. Caselli & Ceccarelli 2012; Ceccarelli et al. 2014; Drozdovskaya et al. 2018). Particularly important is understanding the possible heritage of iCOMs, for the hypothetical link with the life emergence on the Earth.

Fig. 5 shows the abundance ratio of the iCOMs detected in SVS13-A and the four comets where some of the same molecules were detected: Hale-Bopp, Lemmon, Lovejoy, and 67P. In the latter, measurements exist of the winter and summer hemispheres (Le Roy et al. 2015). The first remark is that in the 67P summer hemisphere formamide and methyl formate have the same abundances, normalized to methanol, than in SVS13-A, whereas acetaldehyde is more than a factor 10 more abundant in 67P. A similar trend is present also in the 67P winter hemisphere, with acetaldehyde more abundant than formamide and methyl formate, although the latter abundances are also larger with respect to those in SVS13-A. In the Lemmon and Lovejoy comets, acetaldehyde and formamide are about a constant factor 20 larger than in SVS13-A, while methyl formate is less than a factor 10 larger. In Hale-Bopp the difference with respect to SVS13-A decreases from formamide to acetaldehyde and to methyl formate. For ethanol the abundance ratios obtained in the two comets Lemmon and Lovejoy are higher with respect to what measured in SVS13-A by less than a factor 10.

Therefore, we can conclude that the relative abundances of methyl formate and ethanol do not seem to be substantially different between SVS13-A and comets within a factor 10. Acetaldehyde shows instead higher relative abundances in comets, while formamide shows the highest spread.

5.4 The case of methoxy

The unprecedented results provided by ASAI, i.e. a large number of iCOMs detected through a large number of emission lines put severe constraints on the iCOMs relative abundances. An interesting case

[8]Note that these are the only Class 0 hot corinos in the literature where all the six iCOMs detected in SVS13-A are available and observed with an interferometer.

Downloaded from https://academic.oup.com/mnras/article/483/2/1850/5174973 by Biblioteca di Scienze, Università degli studi di Firenze user on 29 December 2020

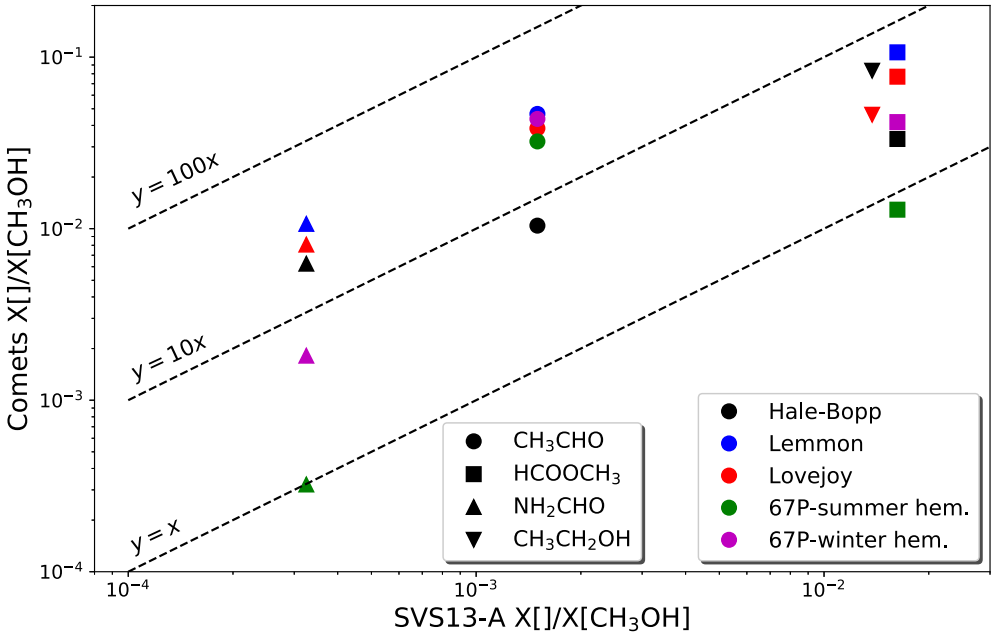


Figure 5. Abundances, normalized to methanol, of the iCOMs detected in various comets (*y*-axis) and SVS-13A (*x*-axis). The different symbols represent different molecules, as marked in the figure inset: acetaldehyde (circles), methyl formate (squares), formamide (up-triangles), and ethanol (low-triangles). The different colours correspond to different comets: Hale-Bopp (black), Lemmon (blue), Lovejoy (red), and 67P in the summer (green) and winter (magenta) hemisphere, respectively. The iCOMs abundances in comets are taken from the compilation of Le Roy et al. (2015), except for ethanol which is from Biver et al. (2015), while the SVS13-A abundances are from this work.

is represented by methoxy (CH_3O), which is not detected in SVS13-A, with an upper limit in the column density of $\leq 3 \times 10^{15}$ cm^{-2}. Similarly, methoxy is not detected in the 'warm sources' observed with the IRAM-NOEMA interferometer[9] within the SOLIS project (*https://solis.osug.fr/*: Ceccarelli et al. 2017), while it is, so far, only detected towards few cold sources (e.g. Cernicharo et al. 2012; Bacmann & Faure 2016; Jiménez-Serra et al. 2016).

Methoxy was recently proposed as a possible precursor of methyl formate and dimethyl ether in gas-phase processes (Balucani et al. 2015). Given the high abundances of $HCOOCH_3$ ($N_{tot} \sim 1.3 \times 10^{17}$ cm^{-2}) and CH_3OCH_3 ($N_{tot} \sim 1.4 \times 10^{17}$ cm^{-2}), the present CH_3O non-detection seems at odds with the proposed gas formation route. However, the low methoxy abundance with respect to that of methyl formate and dimethyl ether may just indicate that all methoxy is consumed to form these two species.

So far, only models adapted to cold objects were published (Balucani et al. 2015; Vasyunin et al. 2017), so that in order to reach firm conclusions, new models adapted to describe hot corino should be considered. These models will have to account for the upper limits here found: $[CH_3O]/[HCOOCH_3]$ and $[CH_3O]/[CH_3OCH_3] < 0.02$.

6 CONCLUSIONS

The analysis of the Class I object SVS13-A provides us the opportunity to characterize the chemical content of a more evolved source, trying to determine a possible evolutionary trend in the comparison with Class 0 protostars. Even if the angular resolution of single-dish data is not enough to disentangle the protostellar components, the large number of lines provided by unbiased spectral surveys (such as ASAI) allows us to analyse the global chemical complexity in a source previously unexplored. Note that we previously (Bianchi et al. 2017a) measured towards SVS13-A a methanol and formaldehyde deuteration up to two orders of magnitude lower than the values measured in Class 0 sources located in the same star-forming region and observed using the same telescope. This was indeed the first indication of a modified chemical content possibly due to the different evolutionary stages. Due to the wide observed bandwidth, we detected several iCOMs such as CH_3CHO, $HCOOCH_3$, CH_3OCH_3, and CH_3CH_2OH, typical of a hot corino. SVS13-A appears to be as chemically rich as previously studied Class 0 protostars. In addition, it seems that the iCOMs abundances do not significantly vary during the protostellar phase. On the other hand, the comparison of the relative iCOMs abundances measured towards SVS13-A and in comets shows different behaviours. More specifically, methyl formate and ethanol do not seem to be substantially different, within a factor 10, in SVS13-A and comets, while for the other iCOMs the difference is larger up to a factor 30.

[9] *http://www.iram-institute.org/*

ACKNOWLEDGEMENTS

The authors are grateful to the IRAM staff for its help in the calibration of the 30-m data. The research leading to these results has received funding from the European Commission Seventh Framework Programme (FP/2007-2013) under grant agreement N 283393 (RadioNet3). This work was supported by by the MIUR (Italian Ministero dell'Istruzione, Università e Ricerca) through the grants: Progetti Premiali 2012 – iALMA (CUP C52I13000140001), the program PRIN-MIUR 2015 STARS in the CAOS (Simulation Tools for Astrochemical Reactivity and Spectroscopy in the Cyberinfrastructure for Astrochemical Organic Species) (2015F59J3R)e). This project has also been supported by the PRIN-INAF 2016 'The Cradle of Life – GENESIS-SKA (General Conditions in Early Planetary Systems for the rise of life with SKA)'. RB acknowledges the fi-

Downloaded from https://academic.oup.com/mnras/article/483/2/1850/5174973 by Biblioteca di Scienze, Università degli studi di Firenze user on 29 December 2020

nancial support from Spanish MINECO (through project FIS2012-32096). Finally, we acknowledge the funding from the European Research Council (ERC) under the European Union's Horizon 2020 research and innovation programme, for the Project 'The Dawn of Organic Chemistry' (DOC), grant agreement No 741002.

REFERENCES

Anglada G., Rodríguez L. F., Torrelles J. M., 2000, ApJ, 542, L123
Arce H. G., Santiago-García J., Jørgensen J. K., Tafalla M., Bachiller R., 2008, ApJ, 681, L21
Avenhaus H. et al., 2018, ApJ, 863, 44
Bachiller R., Guilloteau S., Gueth F., Tafalla M., Dutrey A., Codella C., Castets A., 1998, A&A, 339, L49
Bacmann A., Faure A., 2016, A&A, 587, A130
Bacmann A., Taquet V., Faure A., Kahane C., Ceccarelli C., 2012, A&A, 541, L12
Balucani N., Ceccarelli C., Taquet V., 2015, MNRAS, 449, L16
Bennett C. J., Kaiser R. I., 2007, ApJ, 661, 899
Bergner J. B., Öberg K. I., Garrod R. T., Graninger D. M., 2017, ApJ, 841, 120
Bianchi E. et al., 2017a, MNRAS, 467, 3011
Bianchi E. et al., 2017b, A&A, 606, L7
Biver N. et al., 2015, Sci. Adv., 1, 1500863
Bottinelli S., Ceccarelli C., Williams J. P., Lefloch B., 2007, A&A, 463, 601
Bottinelli S. et al., 2004, ApJ, 615, 354
Brown R. D., Crofts J. G., Godfrey P. D., Gardner F. F., Robinson B. J., Whiteoak J. B., 1975, ApJ, 197, L29
Caselli P., Ceccarelli C., 2012, Astron. Astrophys. Rev., 20, 56
Cazaux S., Tielens A. G. G. M., Ceccarelli C., Castets A., Wakelam V., Caux E., Parise B., Teyssier D., 2003, ApJ, 593, L51
Ceccarelli C., Caselli P., Bockelée-Morvan D., Mousis O., Pizzarello S., Robert F., Semenov D., 2014, in Henrik B., Ralf S. K., Cornelis P. D., Thomas H., eds, Protostars and Planets VI. University of Arizona Press, Tucson, p. 859
Ceccarelli C., Caselli P., Herbst E., Tielens A. G. G. M., Caux E., 2007, in Reipurth B., Jewitt D., Keil K., eds, Protostars and Planets V. University of Arizona Press, Tucson, p. 47
Ceccarelli C. et al., 2017, ApJ, 850, 176
Cernicharo J., Marcelino N., Roueff E., Gerin M., Jiménez-Escobar A., Muñoz Caro G. M., 2012, ApJ, 759, L43
Chapillon E. et al., 2012, ApJ, 756, 58
Charnley S. B., 2004, Adv. Space Res., 33, 23
Charnley S. B., Tielens A. G. G. M., Millar T. J., 1992, ApJ, 399, L71
Charnley S. B., Tielens A. G. G. M., Rodgers S. D., 1997, ApJ, 482, L203
Chen X., Launhardt R., Henning T., 2009, ApJ, 691, 1729
Chini R., Reipurth B., Sievers A., Ward-Thompson D., Haslam C. G. T., Kreysa E., Lemke R., 1997, A&A, 325, 542
Chuang K.-J., Fedoseev G., Qasim D., Ioppolo S., van Dishoeck E. F., Linnartz H., 2017, MNRAS, 467, 2552
Codella C., Bachiller R., Reipurth B., 1999, A&A, 343, 585
Codella C., Fontani F., Ceccarelli C., Podio L., Viti S., Bachiller R., Benedettini M., Lefloch B., 2015, MNRAS, 449, L11
Codella C. et al., 2010, A&A, 518, L112
Codella C. et al., 2014, A&A, 568, L5
Codella C. et al., 2016, A&A, 586, L3
Codella C. et al., 2017, A&A, 605, L3
Codella C. et al., 2018, A&A, 617, A10
Coutens A. et al., 2016, A&A, 590, L6
Cuppen H. M., Walsh C., Lamberts T., Semenov D., Garrod R. T., Penteado E. M., Ioppolo S., 2017, Space Sci. Rev., 212, 1
De Simone M. et al., 2017, A&A, 599, A121
Drozdovskaya M. N. et al., 2018, MNRAS, 476, 4949
Dutrey A. et al., 2014, Nature, 514, 600
Enoch M. L., Corder S., Dunham M. M., Duchêne G., 2009, ApJ, 707, 103
Enrique-Romero J., Rimola A., Ceccarelli C., Balucani N., 2016, MNRAS, 459, L6
Favre C. et al., 2018, ApJ, 862, L2
Garrod R. T., Herbst E., 2006, A&A, 457, 927
Garrod R. T., Widicus Weaver S. L., Herbst E., 2008, ApJ, 682, 283
Garufi A. et al., 2017, The Messenger, 169, 32
Gerin M., Pety J., Fuente A., Cernicharo J., Commerçon B., Marcelino N., 2015, A&A, 577, L2
Graninger D. M., Wilkins O. H., Öberg K. I., 2016, ApJ, 819, 140
Herbst E., van Dishoeck E. F., 2009, ARA&A, 47, 427
Hirota T. et al., 2008, PASJ, 60, 37
Hollis J. M., Vogel S. N., Snyder L. E., Jewell P. R., Lovas F. J., 2001, ApJ, 554, L81
Hudson R. L., Loeffler M. J., 2013, ApJ, 773, 109
Imai M. et al., 2016, ApJ, 830, L37
Jaber A. A., Ceccarelli C., Kahane C., Caux E., 2014, ApJ, 791, 29
Jiménez-Serra I. et al., 2016, ApJ, 830, L6
Jørgensen J. K., Favre C., Bisschop S. E., Bourke T. L., van Dishoeck E. F., Schmalzl M., 2012, ApJ, 757, L4
Jørgensen J. K. et al., 2016, A&A, 595, A117
Jørgensen J. K. et al., 2018, A&A, in press
Kahane C., Ceccarelli C., Faure A., Caux E., 2013, ApJ, 763, L38
Laas J. C., Garrod R. T., Herbst E., Widicus Weaver S. L., 2011, ApJ, 728, 71
Lattelais M., Pauzat F., Ellinger Y., Ceccarelli C., 2009, ApJ, 696, L133
Lefloch B., Castets A., Cernicharo J., Langer W. D., Zylka R., 1998, A&A, 334, 269
Lefloch B., Ceccarelli C., Codella C., Favre C., Podio L., Vastel C., Viti S., Bachiller R., 2017, MNRAS, 469, L73
Lefloch B. et al., 2018, MNRAS, 477, 4792
Lefèvre C. et al., 2017, A&A, 604, L1
Le Roy L. et al., 2015, A&A, 583, A1
Looney L. W., Mundy L. G., Welch W. J., 2000, ApJ, 529, 477
López-Sepulcre A. et al., 2015, MNRAS, 449, 2438
López-Sepulcre A. et al., 2017, A&A, 606, A121
Maury A. J. et al., 2014, A&A, 563, L2
Mendoza E., Lefloch B., López-Sepulcre A., Ceccarelli C., Codella C., Boechat-Roberty H. M., Bachiller R., 2014, MNRAS, 445, 151
Myers P. C., Adams F. C., Chen H., Schaff E., 1998, ApJ, 492, 703
Myers R. J., Bright Wilson E., Jr., 1960, J. Chem. Phys., 33, 186
Müller H. S. P., Schlöder F., Stutzki J., Winnewisser G., 2005, J. Mol. Struct., 742, 215
Müller H. S. P., Thorwirth S., Roth D. A., Winnewisser G., 2001, A&A, 370, L49
Neill J. L. et al., 2012, ApJ, 755, 153
Ohishi M., Kawaguchi K., Kaifu N., Irvine W. M., Minh Y. C., Yamamoto S., Saito S., 1991, in Haschick A. D., Ho P. T. P., eds, ASP Conf. Ser., Vol. 16. Ions and Molecules: New Results in Spectral Line Astrophysics, Astron. Soc. Pac., San Francisco, p. 387
Ospina Zamudio J., Lefloch B., Ceccarelli C., Kahane C., Favre C., López-Sepulcre A., Montarges M., 2018, A&A, 618, 145
Oya Y. et al., 2017, ApJ, 837, 174
Öberg K. I., Guzmán V. V., Furuya K., Qi C., Aikawa Y., Andrews S. M., Loomis R., Wilner D. J., 2015, Nature, 520, 198
Öberg K. I., Lauck T., Graninger D., 2014, ApJ, 788, 68
Öberg K. I., van der Marel N., Kristensen L. E., van Dishoeck E. F., 2011, ApJ, 740, 14
Pearson J. C., Brauer C. S., Drouin B. J., 2008, J. Mol. Spectrosc., 251, 394
Pezzuto S. et al., 2012, A&A, 547, A54
Pickett H. M., Poynter R. L., Cohen E. A., Delitsky M. L., Pearson J. C., Müller H. S. P., 1998, J. Quant. Spectrosc. Radiat. Transfer, 60, 883
Reipurth B., Chini R., Krugel E., Kreysa E., Sievers A., 1993, A&A, 273, 221
Rodríguez L. F., Anglada G., Curiel S., 1999, ApJS, 125, 427
Rubin R. H., Swenson G. W., Jr., Benson R. C., Tigelaar H. L., Flygare W. H., 1971, ApJ, 169, L39
Saladino R., Botta G., Pino S., Costanzo G., Di Mauro E., 2012, Chem. Soc. Rev., 41, 5526
Skouteris D., Balucani N., Ceccarelli C., 2019, MNRAS, 482, 3567

Downloaded from https://academic.oup.com/mnras/article/483/2/1850/5174973 by Biblioteca di Scienze, Università degli studi di Firenze user on 29 December 2020

Skouteris D., Balucani N., Ceccarelli C., Vazart F., Puzzarini C., Barone V., Codella C., Lefloch B., 2018, ApJ, 854, 135
Skouteris D., Vazart F., Ceccarelli C., Balucani N., Puzzarini C., Barone V., 2017, MNRAS, 468, L1
Snyder L. E., Buhl D., Schwartz P. R., Clark F. O., Johnson D. R., Lovas F. J., Giguere P. T., 1974, ApJ, 191, L79
Taquet V., López-Sepulcre A., Ceccarelli C., Neri R., Kahane C., Charnley S. B., 2015, ApJ, 804, 81
Taquet V., Wirström E. S., Charnley S. B., 2016, ApJ, 821, 46
Taquet V., Wirström E. S., Charnley S. B., Faure A., López-Sepulcre A., Persson C. M., 2017, A&A, 607, A20
Tobin J. J. et al., 2015, ApJ, 805, 125
Tobin J. J. et al., 2016, ApJ, 818, 73
Turner B. E., 1977, ApJ, 213, L75
Turner B. E., 1991, ApJS, 76, 617
Vastel C., Ceccarelli C., Lefloch B., Bachiller R., 2014, ApJ, 795, L2
Vasyunin A. I., Caselli P., Dulieu F., Jiménez-Serra I., 2017, ApJ, 842, 33
Walsh C. et al., 2016, ApJ, 823, L10
Yamaguchi T. et al., 2012, PASJ, 64, 105
Zuckerman B. et al., 1975, ApJ, 196, L99

SUPPORTING INFORMATION

Supplementary data are available at *MNRAS* online.

Appendix A. Rotational diagram analysis.
Appendix B. Ethanol: quantum chemistry computation.
Appendix C. iCOMs spectra and tables.

Please note: Oxford University Press is not responsible for the content or functionality of any supporting materials supplied by the authors. Any queries (other than missing material) should be directed to the corresponding author for the article.

This paper has been typeset from a TEX/LATEX file prepared by the author.

Downloaded from https://academic.oup.com/mnras/article/483/2/1850/5174973 by Biblioteca di Scienze, Università degli studi di Firenze user on 29 December 2020